Reliability of CHAMP Anomaly Continuations

Ralph R.B. von Frese[1], Hyung Rae Kim[2], Patrick T. Taylor[3], and Mohammad F. Asgharzadeh[1]

[1] Dept. of Geological Sciences, The Ohio State University, Columbus, OH, USA vonfrese@osu.edu
[2] UMBC/GEST and Geodynamics Branch, NASA/GSFC, Greenbelt, MD, USA
[3] Geodynamics Branch, NASA/GSFC, Greenbelt, MD, USA

Summary: CHAMP is recording state-of-the-art magnetic and gravity field observations at altitudes ranging over roughly 300 - 550 km. However, anomaly continuation is severely limited by the non-uniqueness of the process and satellite anomaly errors. Indeed, our numerical anomaly simulations from satellite to airborne altitudes show that effective downward continuations of the CHAMP data are restricted to within approximately 50 km of the observation altitudes while upward continuations can be effective over a somewhat larger altitude range. The great unreliability of downward continuation requires that the satellite geopotential observations must be analyzed at satellite altitudes if the anomaly details are to be exploited most fully. Given current anomaly error levels, joint inversion of satellite and near-surface anomalies is the best approach for implementing satellite geopotential observations for subsurface studies. We demonstrate the power of this approach using a crustal model constrained by joint inversions of near-surface and satellite magnetic and gravity observations for Maud Rise, Antarctica, in the southwestern Indian Ocean. Our modeling suggests that the dominant satellite altitude magnetic anomalies are produced by crustal thickness variations and remanent magnetization of the normal polarity Cretaceous Quiet Zone.

Key words: satellite magnetic and gravity anomaly continuation, Maude Rise, Antarctica, ADMAP, CHAMP, Ørsted.

1 Introduction

Satellite magnetic and gravity observations are commonly represented by geopotential models that are interrogated for anomaly estimates at or near the Earth's surface. For example, downward continued satellite magnetic anomalies have been compared with aeromagnetic anomalies (e.g., [1]), recommended for leveling aeromagnetic datasets with disparate survey parameters into regional anomaly compilations (e.g., [2]), and used to infer the magnetic field at the core-mantle boundary (e.g., [3]). Geological applications of satellite gravity observations also typically evaluate the anomalies at or near the Earth's surface (e.g., [4]).

However, as shown in the sections below, anomaly errors severely limit these applications. For example, just the satellite measurement errors alone restrict viable anomaly continuations to within roughly +/- 50 km of mission altitude. The non-uniqueness of anomaly continuation also confines satellite geopotential anomaly analyses to a very restricted range of altitudes about the mission observations. Hence, for improved understanding of the geopotential fields below mission altitude, lower altitude surveying is necessary from shipborne, airborne, balloon, space shuttle, and space station platforms. As shown below, joint inversion can combine the low-altitude and satellite observations for greatly improved, but not unique estimates of the intervening anomaly fields.

2 Spherical prism anomaly simulations

We illustrate the results described above using the spherical prism magnetic anomaly simulations in Figure 1, which can be directly extended to comparable gravity anomaly simulations by Poisson's relation (e.g., [5]). The left column in Figure 1 gives the total magnetic field anomalies for five arbitrary crustal prisms modeled to 16-decimal place accuracy directly in spherical coordinates by Gauss-Legendre quadrature integration [6]. The spherical prisms are outlined and labeled in black with cgs-volume magnetic susceptibility contrasts of 0.0061468 for prism A, - 0.0028831 for B, 0.0009452 for C, 0.0029529 for D, and – 0.0004456 for F. All prisms are 25 km thick with tops at 5 km below sea level. For each map, the observation grid is at Z km above sea level and has 80 nodes at an interval of about 77 km over the Balkan test region (35 - 42)°N, (22 - 28)°W. Core field attributes at the source and observation points were evaluated from the Magsat 12/83 model [7] updated to 1980.

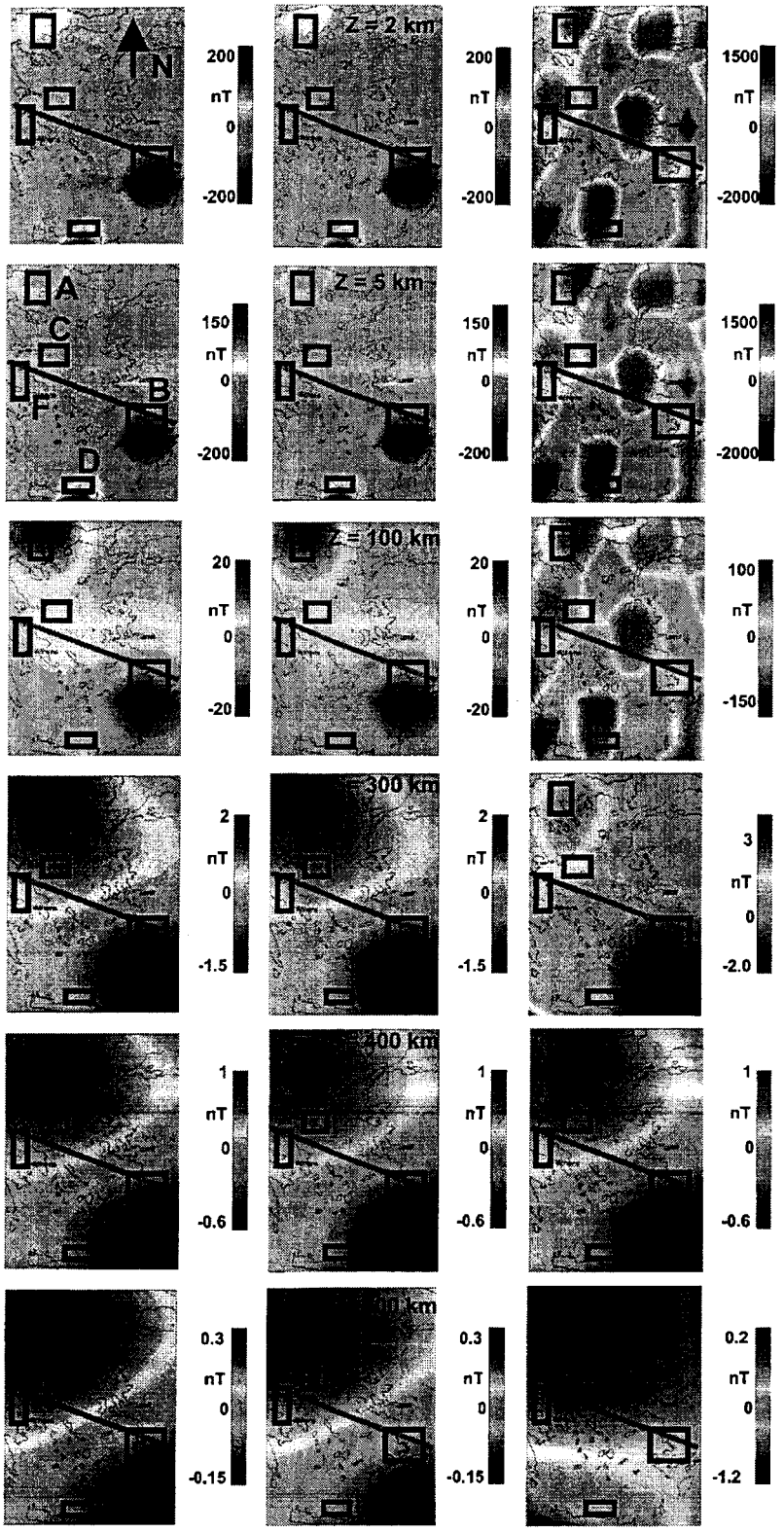

Figure 1: Comparisons of magnetic anomalies for 5 prisms modeled directly in spherical coordinates (left column), the joint inversion of the 5 km and 400 km altitude fields truncated to 0.1 nT accuracy (middle column), and the single inversion of the 400 km altitude field truncated to 0.1 nT (right column).

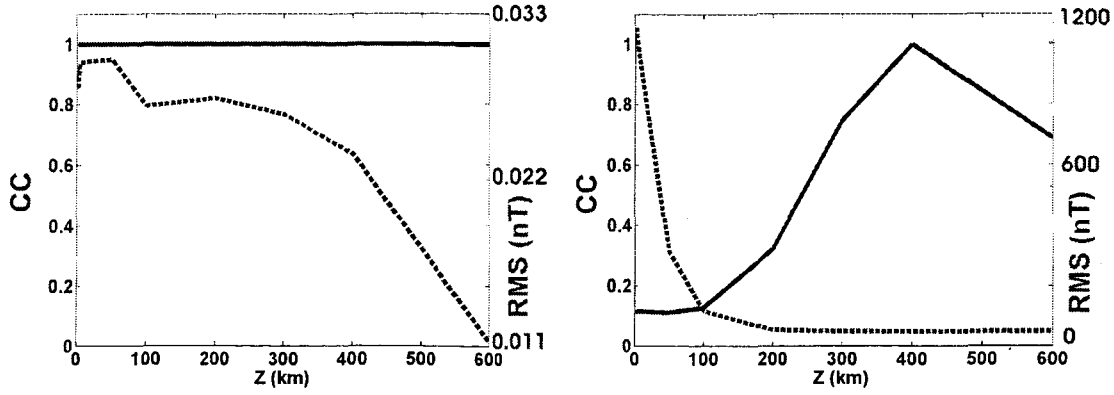

Figure 2: Performance diagrams comparing correlation coefficients (CC) and root-mean-squared differences (RMS) for the anomaly predictions from joint inversion (left), and just the 400 km altitude anomalies truncated to the nearest 0.1 nT (right).

The middle column of Figure 1 shows the great capacity for effective anomaly continuation of the joint inversion of near-surface and satellite altitude data of limited accuracy. Here, we truncated the prism anomalies at altitudes 5 and 400 km to the CHAMP measurement accuracy of 0.1 nT and modeled the truncated anomalies by equivalent point source (EPS) inversion [5] [8] [9]. The EPS grid involved 1079 dipoles located 50 km below sea level at an interval of about 30 km. Comparing the maps of the left and middle columns shows that the EPS anomaly predictions match the prism anomalies remarkably well at all altitudes. The left diagram of Figure 2 generalizes the performance of the joint inversion in terms of the correlation coefficients (CC in the solid profile) and root-mean-squared (RMS) anomaly differences (dotted profile) between the related maps of the two columns.

The right column of Figure 1 gives the marginal results from EPS inversion where only the truncated anomalies at 400 km are considered. These results, which are summarized in Figure 2 by the right performance diagram, show that viable anomaly continuations are essentially restricted to +/- 50 km of the truncated anomalies. Improving the accuracy of the satellite observations only marginally enhances effective anomaly continuation.

Figure 3 illustrates the problem perhaps more insightfully. The top panel shows a vertical slice of the anomaly field from 5 to 200 km altitude at 5 km altitude increments along the NW-SE traverse marked in Figure 1. In the lower right panel, the solid line gives the 200 km anomaly profile to 16-decimal place accuracy at 5 km station intervals that is very close to optimal for trying to recover the 5 km profile in the right panel by downward continuation. However, in practice we estimate satellite anomalies at best to perhaps 1 nT accuracy (blocked profile in the lower right panel) and at stations (dots) with intervals that correspond roughly to the altitude of the observations. Clearly, the restricted accuracy and spatial sampling of satellite anomalies greatly limit the altitude range over which the anomaly continuations are effective.

Furthermore, the veracity of satellite anomalies continued great distances from the observations is very dubious due to the non-uniqueness of anomaly continuation. To see this, we note that the fitting of any model (e.g., spherical harmonics, Fourier transform, equivalent source, etc.) to a set of geopotential observations can be generically expressed by the matrix equation $\mathbf{AX} = \mathbf{B}$, which has the least squares solution $\mathbf{X} = (\mathbf{A}^t\mathbf{A})^{-1}\mathbf{A}^t\mathbf{B}$, where $\mathbf{A}^t$ is the transposed design matrix $\mathbf{A}$, $\mathbf{X}$ the column matrix of solution coefficients, and $\mathbf{B}$ the column matrix of n observations.

For joint inversion of a high- and low-altitude set of observations, the observation vector can be expressed by $\mathbf{B} = \mathbf{B_h} + \mathbf{B_l}$, where $\mathbf{B_h} = (b_{h1}\, b_{h2} \ldots b_{hm}\, 0_{l1}\, 0_{l2} \ldots 0_{lk})^t$ is the high-altitude observation vector, $\mathbf{B_l} = (0_{h1}\, 0_{h2} \ldots 0_{hm}\, b_{l1}\, b_{l2} \ldots b_{lk})^t$ the low-altitude vector, and $n = m + k$. The solution is then given by $\mathbf{X} = (\mathbf{A}^t\mathbf{A})^{-1}\mathbf{A}^t(\mathbf{B_h} + \mathbf{B_l}) = \mathbf{X_h} + \mathbf{X_l}$. Clearly, the partial solutions $\mathbf{X_h}$ and $\mathbf{X_l}$ making up the total solution $\mathbf{X}$ are basically independent of the actually observed anomaly values in $\mathbf{B_l}$ and $\mathbf{B_h}$, respectively. In principle, the anomaly prediction from a given inversion at an unmapped location is not unique because the solution can be extended by superposition to accommodate any anomaly value there.

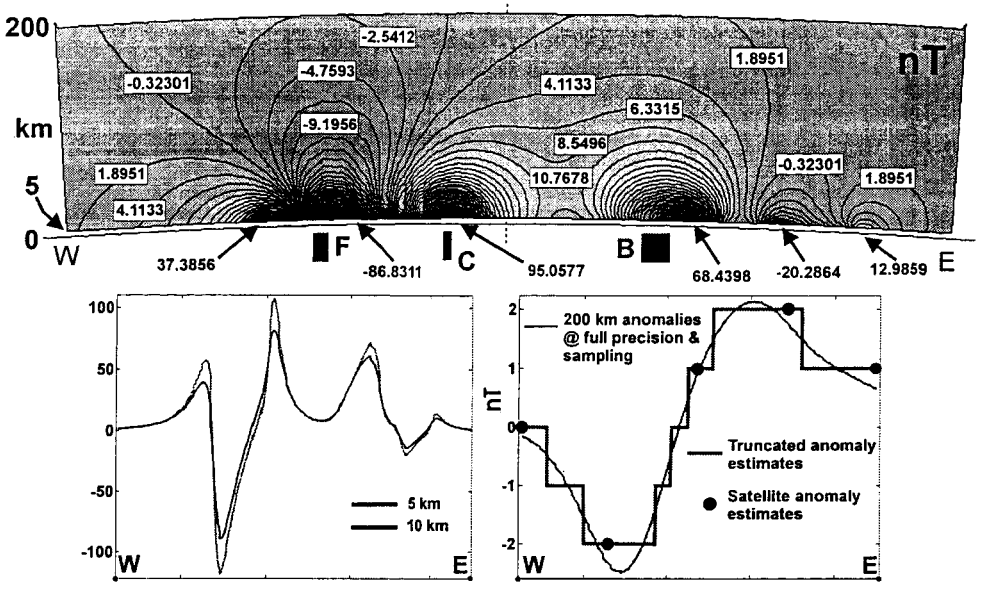

Figure 3: Vertical slice of anomaly values along the profile in Figure 1 between 5 and 200 km altitudes (top) with anomaly comparisons at the 5 and 10 km altitudes (lower left) and at 200 km altitude (lower right).

In practice, the computational limitations of our inversion codes [10] readily admit anomaly prediction ambiguities at distances of about 50 km and greater from the satellite observations. Thus, for the fullest understanding of the anomaly fields between the Earth's surface and satellite altitudes, we really must exploit every opportunity to directly map the lower altitude fields. In the next section, we demonstrate the exciting new dimension of satellite geopotential anomaly interpretation that is offered by this approach.

3 Surface-to-satellite altitude magnetic anomaly variations

For enhanced geological studies of Maude Rise, Antarctica, [11] produced a crustal magnetization model from the joint inversion of magnetic anomalies at 5 km and 700 km altitudes. The 5 km altitude data were low-pass filtered anomalies ($\geq$ 400 km) from the grid of airborne and shipborne magnetic anomalies maintained by the Antarctic Digital Magnetic Anomaly Project [12]. The 700 km altitude anomalies were derived directly from the magnetic observations of the Ørsted mission [13].

Joint inversion of the two anomaly fields obtained a crustal magnetization model with the effects shown in Figure 4 [11]. This magnetization model accounted for thickness variations of the crust as inferred from seismic data supplemented by satellite altitude gravity observations [14], remanent magnetization variations of the oceanic crust, and the variable core field attributes over the study region. Maps A and H of Figure 4 show the modeled effects that match with negligible error the original 5 km and 700 km input anomaly fields, respectively.

Consideration of the model predictions over the intervening altitudes suggests that the dominant magnetic effects at satellite altitudes are from crustal thickness variations and remanence involving the normal polarity Cretaceous Quiet Zone (KQZ). Modeling of the regional components of the residual Ørsted and near-surface magnetic anomalies supports extending the KQZ eastwards from Maude Rise (MR in Figure 4.A) towards the Astrid Ridge (AR), while the higher frequency residual near-surface anomalies can be related to crustal features with effects that are strongly attenuated at satellite altitudes.

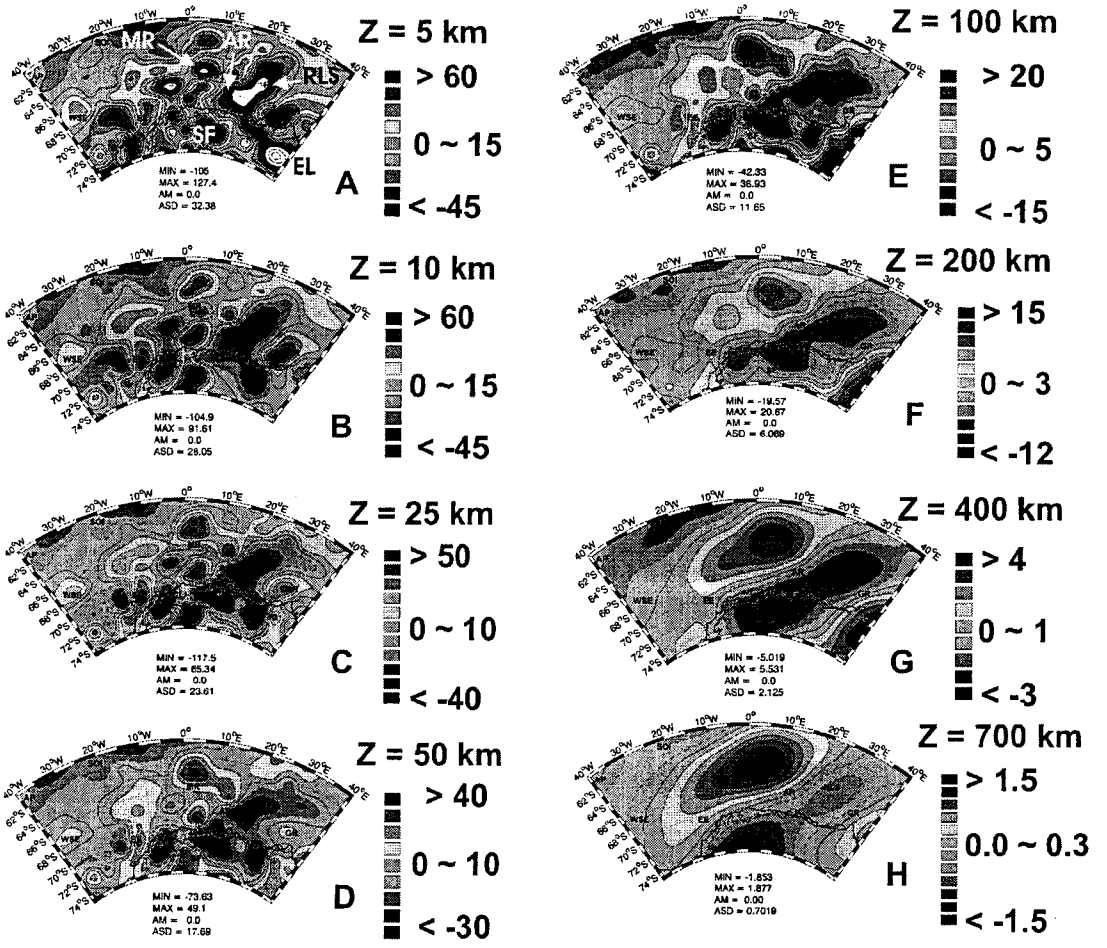

Figure 4: Magnetic anomaly predictions in nT for the Maude Rise region of Antarctica based on the joint inversion of regional ADMAP and Ørsted data at respective altitudes of 5 and 700 km.

The 8 slices of the geomagnetic field evaluated in Figure 4 from the crustal magnetization model provide insight on how the 3 or 4 satellite altitude anomalies break down with decreasing altitude into a complex multitude of anomalies at the near-surface. Alternatively, we can obtain insight on anomaly interference effects with elevation by studying how the near-surface anomalies coalesce with increasing altitude into the roughly handful of anomalies that are observed at satellite altitude.

For example, at the near-surface altitudes (maps A-B) the KQZ is complexly characterized by linear maxima over and along the Maude Rise (MR) with relatively well-defined interior minima. It's only at altitudes of about 100 km and greater (maps E-H) that the strong, regionally positive magnetic character of the KQZ becomes apparent.

Similarly, the near-surface magnetic minima along the coast of East Antarctica coalesce at altitudes of 100 km and higher with the Riiser-Larsen Sea (RLS) minimum. The near-surface continental minima are broken up by a maximum over Sveshjfella (SF) that dies out at altitudes of nearly 200 km and higher. By then, however, the SF anomaly appears to connect with a positive anomaly over western Enderby Land (EL) that may reflect an Archean shield or platform [15]. The EL anomaly is weakly expressed in the near-surface data, but becomes increasingly prominent with altitude.

The anomaly behavior in Figure 4 suggested by the joint inversion clearly would not be revealed in the simple downward continuation of the satellite altitude data nor in the upward continuation of the near-surface magnetic data. Unfortunately, like for any inversion, the results of our joint inversion are not

unique. Thus, they do not obviate the need for supplemental magnetic measurements, especially at the intervening altitudes that may be accessed by high-altitude aircraft, balloons, and space shuttle tethers, to better define the geologic relationships in the near-surface and satellite altitude magnetic fields.

References

1. Sexton J L, W J Hinze, R R B von Frese and L W Braile (1982), Long-wavelength aeromagnetic anomaly map of the conterminous U.S.A., *Geology 10*, 364-369.

2. von Frese R R B, H R Kim, L Tan, J W Kim, P T Taylor, M E Purucker, D E Alsdorf and C A Raymond (1999), Satellite magnetic anomalies of the Antarctic crust, *Annali di Geofisica 42*, 309-326.

3. Gubbins D, and J Bloxham (1985), Geomagnetic field analysis, III, Magnetic fields on the core-mantle boundary, *Geophys. J.R. Astron. Soc. 80*, 695-713.

4. Llubes M, N Florsch, B Legresy, J-M Lemoine, S Loyer, D Crossley and F Rémy (2003), Crustal thickness in Antarctica from CHAMP gravimetery, *Earth Planet. Sci. Lett. 212*, 103-117.

5. von Frese R R B, W J Hinze and L W Braile (1981), Spherical earth gravity and magnetic anomaly analysis by equivalent point source inversion, *Earth Planet. Sci. Lett. 53*, 69-83.

6. von Frese R R B, W J Hinze, L W Braile and A J Luca (1981), Spherical earth gravity and magnetic anomaly modeling by Gauss-Legendre quadrature integration, *J. Geophys. 49*, 234-242.

7. Langel R A, and R H Estes (1985), The near-earth geomagnetic field at 1980 determined from Magsat data, *J. Geophys. Res. 90*, 2,495-2,510.

8. von Frese R R B, D N Ravat, W J Hinze and C A McGue (1988), Improved inversion of geopotential field anomalies for lithospheric investigations, *Geophysics 53*, 375-385.

9. von Frese R R B (1998), Correction to: von Frese R R B, W J Hinze, and L W Braile, Spherical earth gravity and magnetic anomaly analysis by equivalent source inversion (Earth Planet. Sci. Lett., 53, 69-83, 1981), *Earth Planet. Sci. Lett. 163*, 409-411.

10. Alsdorf D E, and R R B von Frese (1994), Fortran Programs for Processing Magsat Data for Lithospheric, External Field and Residual Core Components, *NASA-GSFC TM104612*, 196 pp..

11. Kim H R, Antarctic Lithospheric Anomalies from Ørsted Satellite and Near-Surface Magnetic Observations (2002), *Ph.D. Dissertation (unpubl.)*, The Ohio State University, Columbus, 160 pp.

12. Golynsky A, M Chiappini, D Damaske, F Ferraccioli, J Ferris, C Finn, M Ghidella, T Isihara, A Johnson, H R Kim, L Kovacs, J LaBrecque, V Masolov, Y Nogi, M Purucker, P Taylor and M Torta (2001), ADMAP – Magnetic Anomaly Map of the Antarctic, 1:10,000,000 scale map, in Morris P, and R von Frese, eds., *BAS (Misc.) 10*, Cambridge, British Antarctic Survey.

13. Kim H R, R R B von Frese, J W Kim, P T Taylor, M E Purucker and T Neubert (2002), Ørsted verifies regional magnetic anomalies of the Antarctic lithosphere, *Geophys. Res. Lett. 29(#15)*, ORS 3-1 to 3-3.

14. von Frese R R B, L Tan, J W Kim and C R Bentley (1999), Antarctic crustal modeling from the spectral correlation of free-air gravity anomalies with the terrain, *J. Geophys. Res. 104*, 25275-25296.

15. Bormann P, P Bankwitz, E Bankwitz, V Damm, E Hurtig, H Kompf, M Menning, H-J Paech, U Schofer and W Stackegrandt (1986), Structure and development of the passive continental margin across the Princess Astrid coast, East Antarctica, *J. Geodyn. 6*, 347-373.